Received 12 January 2021; revised 5 February 2021; accepted 5 February 2021. Date of publication 16 February 2021; date of current version 8 March 2021.

Digital Object Identifier 10.1109/OJAP.2021.3059501

RF-Powered Wearable Energy Harvesting and Storage Module Based on E-Textile Coplanar Waveguide Rectenna and Supercapacitor

MAHMOUD WAGIH (Graduate Student Member, IEEE), NICHOLAS HILLIER, SHENG YONG, ALEX S. WEDDELL (Member, IEEE), AND STEVE BEEBY (Senior Member, IEEE)

School of Electronics and Computer science, University of Southampton, Southampton SO17 1BJ, U.K.

CORRESPONDING AUTHOR: M. WAGIH (e-mail: mahm1g15@ecs.soton.ac.uk)

This work was supported in part by the European Commission through the Project EnABLES, funded under H2020-EU.1.4.1.2 under Grant 730957, and in part by U.K. Engineering and Physical Sciences Research Council (EPSRC) under Grant EP/P010164/1 and Grant EP/L016818/1.

ABSTRACT This paper presents a high-efficiency compact ($0.016\lambda_0^2$) textile-integrated energy harvesting and storage module for RF power transfer. A flexible 50 μm-thick coplanar waveguide rectenna filament is integrated with a spray-coated supercapacitor to realize an "e-textile" energy supply module. The meandered antenna maintains an $S_{11} < -6$ dB inside and outside the fabric and in human proximity with a 2.3 dBi gain. The rectifier achieves a peak RF-DC efficiency of 80%, across a 4.5 kΩ load, and a 1.8 V open-circuit voltage from -7 dBm. The supercapacitor is directly spray-coated on a cotton substrate using carbon and an aqueous electrolyte. When connected to the supercapacitor, the rectifier achieves over an octave half-power bandwidth. The textile-integrated rectenna is demonstrated charging the supercapacitor to 1.5 V (8.4 mJ) in 4 minutes, at 4.2 m from a license-free source, demonstrating a significant improvement over previous rectennas while eliminating power management circuitry. The integrated module has an end-to-end efficiency of 38% at 1.8 m from the transmitter. On-body, the rectenna's efficiency is 4.8%, inclusive of in-body losses and transient shadowing, harvesting 4 mJ in 32 seconds from 16.6 μW/cm^2. It is concluded that e-textile rectennas are the most efficient method for powering wearables from μW/cm^2 power densities.

INDEX TERMS Antennas, energy harvesting, flexible printed circuits, impedance matching, microstrip antennas, rectennas, rectifiers, supercapacitor, wireless power transmission.

I. INTRODUCTION

ELECTRONIC-TEXTILES (e-textiles) have attracted significant interest for a variety of wearable sensing and activity tracking applications [1]. Among the requirements of e-textiles is unobtrusive integration with garments [2], and being able to run autonomously using textile-based energy harvesters [3].

Radio Frequency Energy Harvesting (RFEH) and Wireless Power Transmission (WPT) using textile-based rectennas represent sustainable methods of continuously providing power to wearable devices. Textile rectennas have been developed from UHF to mmWave bands using broadside and omnidirectional antennas [4]–[9]. Nevertheless, the reported rectennas have only been investigated as continuous power sources, and characterized in their steady-state. However, a wearable antenna is susceptible to polarization misalignments, additional path losses, and body shadowing [10], which affects the RFEH performance of a rectenna [11]. For instance, when harvesting from a GSM phone, movements in the range of 7 to 20 cm away from the phone can alter the harvested power by a factor of 5 [12]. Therefore, for RF-powered e-textiles to be fully-realized, integration with body-friendly textile-based energy storage devices is crucial.

The research interest in textile and wearable supercapacitors has seen a significant growth over the past decade [13], with two orders of magnitude increase in academic publications in the area. Textile supercapacitors (TSCs) can be broadly separated into two classes of device:

yarn-based [14]–[16] or 2-dimensional layered [17]–[19], with each being demonstrated with a myriad of electrode materials and electrolytes. The most common electrode materials are porous carbon, 2D materials, transition metal oxides and conductive polymers [20]. With long cycle life, fast charging and discharging rates and good energy density, TSCs are seen as a complementary technology to energy harvesters to enable battery-less e-textiles. Applied to RFEH, TSCs overcome the intermittency in the power delivered by a wearable rectenna due to body-shadowing and movement, in addition to buffering the energy for power-intensive applications.

System-level investigations of rectennas integrated with energy storage devices have previously been presented. For example, rectennas were interfaced with a commercial boost converter Power Management Integrated Circuit (PMIC) [21]–[24]. In [22], a sensor node was powered using a 7 mF commercial supercapacitor following 8 minutes of charging from an incident RF power density of 12.6 μW/cm^2. In [4], a textile-based rectifier was characterized while charging a 1.3 mF electrolytic capacitor. A railway monitoring sensor node was proposed in [25] using a rectenna integrated with an electrolytic capacitor and a buck converter with up to 2 m range. A 3D-printed enclosure combining RFEH with a solar cell was used to charge an electrolytic capacitor through a boost converter IC was presented in [24] for sub-μW/cm^2 power densities. A flexible battery was reported in [26] with an 11.6% average charging efficiency from a PCB rectenna at 0.5 m distance from a license-free transmitter. In e-textiles, mechanical ferroelectric and triboelectric energy harvesters were also demonstrated directly charging TSCs for wearable applications [27], [28]. Nevertheless, the end-to-end efficiency of such systems does not exceed 1% due to the high impedance of the harvester.

In this paper, an e-textile RFEH and storage module is proposed for wearable applications, capable of harvesting 8.4 mJ in under 4 minutes, at 4.2 m from an Industrial Scientific Medical (ISM)-band 915 MHz source. In [29], we introduced the concept of a textile energy storage device integrated with a rectenna, achieving 15% charging efficiency at 1.2 m from a transmitter. Nevertheless, detailed antenna design, wearable performance, large-signal charging efficiency, and operation range were not investigated, where it was previously shown that human proximity can reduce the antenna's gain by at least 3 dB reducing the harvested power by multiple factors [4]. Moreover, the rectifier in [29] was not tailored towards a TSC as a load. In Section II, the design methodology for an e-textile RFEH module is introduced and contrasted to existing rectennas integrated with energy storage devices. The design and characterization of a wearable Coplanar-Waveguide (CPW) rectenna filament is presented in Section III. The implementation and characterization of the TSC is then presented in Section IV. The rectifier's performance when integrated with the TSC is analyzed experimentally using DC and RF techniques in Section V. Finally, the wireless performance of the rectenna is evaluated in a license-free ISM-band WPT application in Section VI, and compared to similar work showing the highest reported end-to-end efficiency.

TABLE 1. Comparison of rectennas integrated with energy storage.

	Implementation	Component count	Peak η
[21]	Planar and 3D rectenna with a commercial PMIC and SC	>20*	1.7%‡
[23]	PCB rectenna with a commercial PMIC and SC	>20*	1.8%‡
[24]	3D-printed rectenna with a commercial PMIC and Capacitor	>20*	1.2%‡
[26]	PCB rectenna + custom CMOS boost converter and flexible battery	≈23**	12%†
[25]	PCB rectenna + whip antenna with a commercial PMIC and SC	≈45**	25%†
This work	**Textile-integrated rectenna and supercapacitor with no PMIC**	**5**	**38%†**

*Based on the PMIC datasheet; **estimated from circuit photograph; † >1μW/cm^2 rectenna; ‡ <1μW/cm^2 rectenna; SC: supercapacitor.

II. CONCEALED E-TEXTILE RF ENERGY HARVESTING AND STORAGE MODULE

The requirements for compact e-textile filaments include being implemented on a thin and flexible substrate, maintaining a narrow width (<1 cm), and containing a small number of miniaturized lumped components, not to reduce the flexibility and user-friendliness of the textile [2]. The circuit filaments can then be encapsulated for improved reliability and woven into the fabric for concealed integration [30]. Examples of previously reported e-textile systems are washable UHF RFID tags based on narrow dipole antennas [30], and accelerometers [31]. In [32], a CPW antenna was proposed on a thin and flexible filament for e-textile RFEH. However, its performance as a rectenna was not investigated, and its wearable performance is susceptible to detuning in human proximity.

The techniques reported in [21]–[26] to realize rectennas integrated with energy storage devices, based on an intermediate supercapacitor/battery-charging PMICs, are not well-suited to wearable e-textiles. To explain, a PMIC such as the TI BQ25504, used in [21]–[24] or the Linear LTC3588 [25], require over 10 lumped components, along with a complex PCB layout to function correctly. Such designs are not wearable-friendly and cannot be integrated in compact and unobtrusive e-textiles. η. Omitting the PMIC would result in the transient current draw of a charging supercapacitor affecting the rectenna's instantaneous PCE and subsequently η. This may result in an impedance mismatch between the rectifier and the DC load being of a lower impedance (i.e., drawing more current). However, as PMIC's do have a considerable active power consumption, and may not be designed to specifically achieve an input impedance within a rectenna's optimal load range.

In Table 1, recent rectenna implementations charging an energy storage device are summarized based on the complexity of their implementation, in terms of components count,

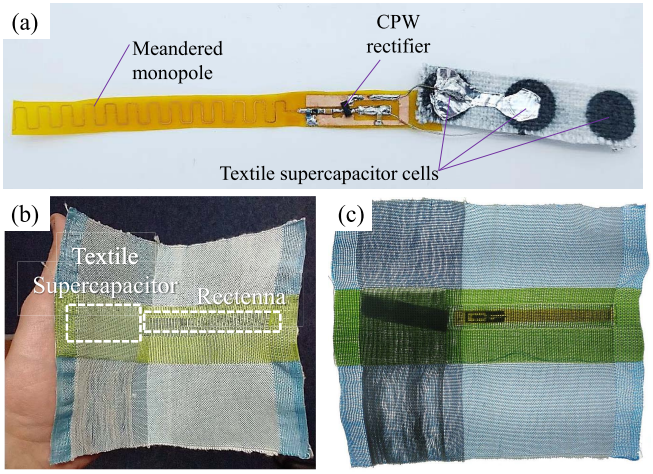

FIGURE 1. Photographs of the proposed integrated e-textile RF energy harvester and storage module: (a) the rectenna filament and encapsulated textile supercapacitor (dimensions in mm); (b) the concealed system in fabric; (c) components of the system visible under high exposure.

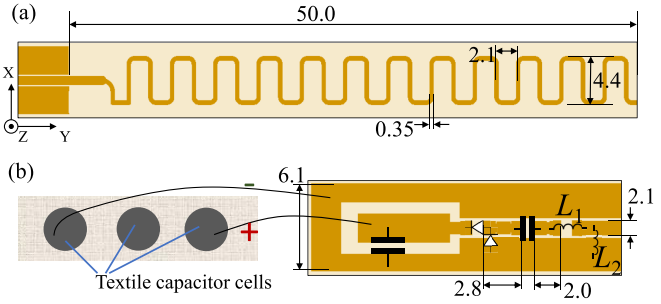

FIGURE 2. Layout and dimensions (in mm) of the meandered CPW antenna filament (a) and the compact voltage doubler rectifier (b).

and the maximum end-to-end RFEH efficiency. As observed in the peak η and the component count, the proposed rectenna achieves the highest end-to-end charging efficiency, as well as maintains the lowest complexity owing to the omission of the intermediate power management stage.

The proposed system is shown in Fig. 1. The rectenna is fabricated using photolithography, [30], on a single-sided polyimide copper-laminate with less than 50 μm-thickness. This fabrication method was previously demonstrated as a mean of realizing highly-reliable and reproducible RF components. For example, washable e-textile RFID tags were proposed based on vacuum-formed antenna filaments [30]. Furthermore, a polyimide-on-fabric rectifier was show to withstand at least 200 bending cycles with no degradation in the DC output [4].

The rectenna's DC output is directly connected to the TSC and concealed in fabric pockets as in Fig. 1-b. This integration technique improves the circuit's resilience to bending [2], [4] and washing [30], in addition to not affecting the user's comfort. As presented in Table 1, the proposed rectenna contains only five lumped components, making it suitable for seamless integration in fabrics, as shown in Fig. 1-b and c. The entire system is compact and occupies an area of 11.5×1.5 cm, i.e., $0.016\lambda^2$ when normalized to λ_0^2 at 915 MHz.

III. RECTENNA FILAMENT DESIGN AND CHARACTERIZATION

A. E-TEXTILE CPW ANTENNA DESIGN

In energy harvesting, achieving a small footprint is essential to enable large-area implementations. "Wire" monopole antennas occupy a significantly smaller physical area compared to their effective radiating aperture [33]. Therefore, the rectenna is designed based on a CPW monopole with a miniaturized ground plane. To further reduce the area of the harvester, the length of the monopole was reduced through meandering.

While the meandered CPW antenna design was shown to have a consistent bandwidth in space and in-textiles [32], human-proximity effects have not been considered; the S_{11} response is expected to vary significantly with bending and human proximity. For unisolated monopoles, it is expected that the resonance of the antenna shifts to a lower frequency, due to the high permittivity of tissue compared to air [34]. While it is possible to use a broadband textile antenna to overcome detuning in a sub-1 GHz rectenna [4], sub-1 GHz broadband antennas require large area and cannot be integrated within flexible e-textile filaments which have a width under 10 mm.

The CPW antenna was simulated in CST Microwave Studio to evaluate its impedance bandwidth and radiation properties. A prototype, with a solder-terminated SMA connector attached to the antenna's CPW feed was measured for experimental validation. As flexible polyimide copper laminates withstand temperatures up to 400°, standard assembly methods (reflow/hand-soldering) can be used for both the SMA and the rectifier components. The antenna was measured using a through, open, short, match (TOSM)-calibrated Rohde & Schwarz ZVB4 Vector Network Analyzer (VNA), the same setup and calibration were used for characterizing the rectifier's DC and RF performance.

In human proximity, the antenna's response is expected to detune due to the higher permittivity of the tissue compared to that of air or the substrate. This often shifts the antenna's resonance to a lower frequency [34], [35]. The proposed antenna is tuned using length reduction, a technique used where shielding is impossible, such as in implanted and insole antennas [34], [35]. This shifts the free-space resonance to a higher frequency. Subsequently, when the antenna is used in human proximity, the resonance will shift to the lower, and desired, frequency band. The simulated and measured reflection coefficient (S_{11}) of the antenna is shown in Fig. 3. The shaded region in Fig. 3 shows the crossover between the antenna's -6 dB (VSWR<3) bandwidth in space and when measured on-body, with an approximately 1 mm air gap. Compared to [34] which achieves an S_{11} around -3 dB at its design frequency in space, the proposed

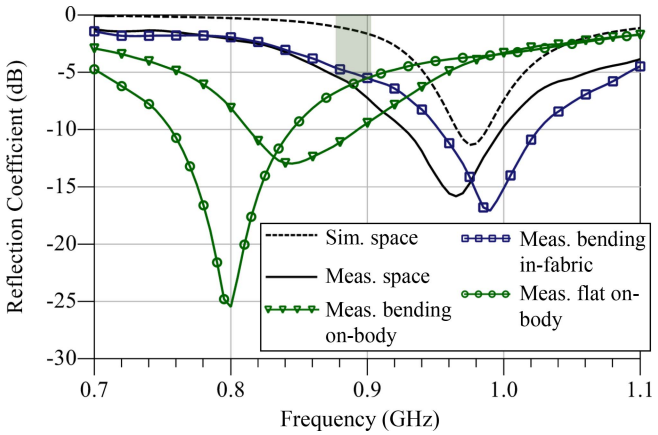

FIGURE 3. Simulated and measured 50 Ω reflection coefficient (S_{11}) of the CPW antenna filament.

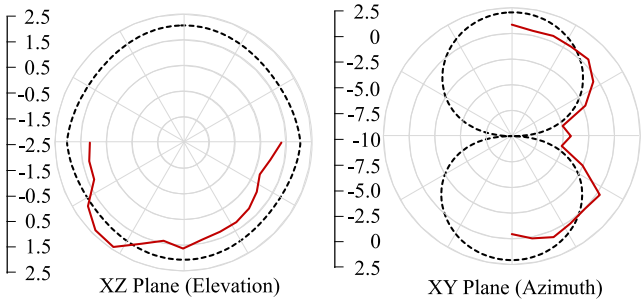

FIGURE 4. Simulated (dashed) and measured (solid) gain patterns of the antenna at 915 MHz.

antenna is able to maintain an $S_{11} < -6$ dB at 915 MHz both in presence and absence of the human body, under flat and bent conditions. When measured inside the fabric, the antenna was bent around a 2 cm radius.

The radiation patterns of the CPW antenna were simulated and measured experimentally. Fig. 4 shows the co-polarized (vertically on the Y-plane) gain patterns of the antenna on the XZ and XY planes. The measured gain was calculated using the free space path loss model at 1.1 m from a 10 dBi log-periodic antenna. The discrepancy between the simulations and measurements is attributed to additional reflection off the SMA connector, which is comparable in size to the CPW feed and the antenna's ground. Nevertheless, it can still be verified that the antenna is predominantly omnidirectional across both the XY and XZ planes. It was previously shown that using omnidirectional rectennas improves the power harvested in wearable operation [36].

B. RECTIFIER DESIGN AND IMPEDANCE MATCHING

The proposed rectifier is based on a voltage doubler topology. This allows the rectifier to reach a higher output voltage level for higher input power levels compared to a single-series [25], which enables faster charging of the supercapactior. The selected diode is the Infineon BAT15-04R,

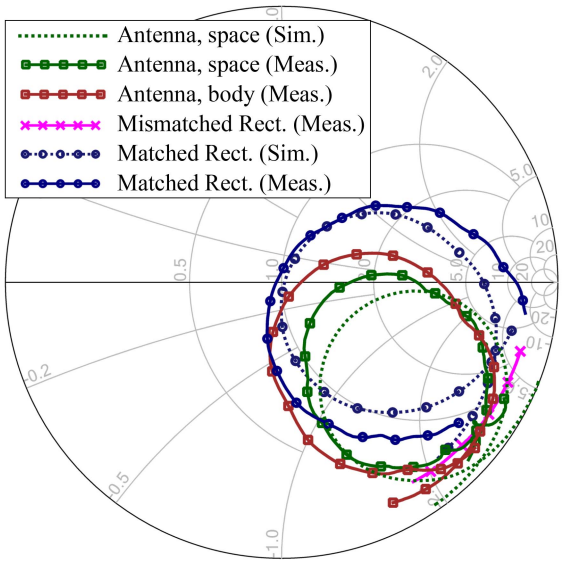

FIGURE 5. Smith chart plot showing the antenna and the rectifier's simulated and measured input impedances, showing the 50 Ω matching.

based on its low forward voltage (0.25 V) and high breakdown voltage (4 V). With two diodes in the same SOT-23 package, the overall component count is reduced.

As the antenna was designed with $Z_0 = 50$ Ω, the rectifier needs to be subsequently matched to the same Z_0. Given the predominantly-capacitive input impedance of rectifiers [4], [37], a series inductor is used for impedance matching. The rectifier's input impedance, before matching, is shown in Fig. 5. By adopting a voltage doubler topology, the equivalent RC circuit of the rectifier has a smaller R and C components, which subsequently enables achieving more broadband performance according to the Bode-Fano bandwidth limit [9], [38]. In addition, as the imaginary component of the rectifier's input impedance is significantly higher than the real component, a higher RF potential will be present at the diode's junction enabling more efficient rectification [39]. The simulated rectifier's optimal input impedance is $20 + j230$ Ω, which can be achieved using a matching network or a co-designed antenna [40]. While a lumped inductor was chosen, implementing the inductor as a distributed microstrip device is possible while maintaining a high PCE as in [41], implemented on a conventional PCB. Nevertheless, a spiral inductor would require a via and a double-sided circuit, increasing the complexity of the fabrication method. As for the Schottky diode, while flexible diodes were proposed for RFEH as high as 2.4 GHz [42], their Power Conversion Efficiency (PCE) is still around 50% lower than the conventional Schottky diodes.

The rectifier matching was optimized in Keysight ADS using harmonic balance simulation, including the CPW layout and the diode's packaging parasitics. Fig. 2-b shows the layout of the CPW rectifier. The selected matching inductor L_1 is a 22 nH wirewound inductor. By opting for a smaller value inductor, the parasitic resistance and capacitance of

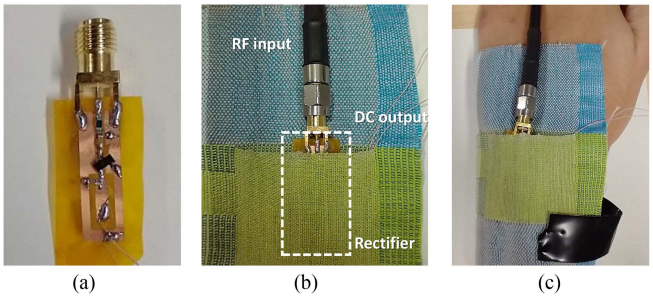

FIGURE 6. Photographs of the connectorized rectifier test setup: (a) rectifier in space; (b) in-fabric "e-etxtile" rectifier; (c) body-worn rectifier.

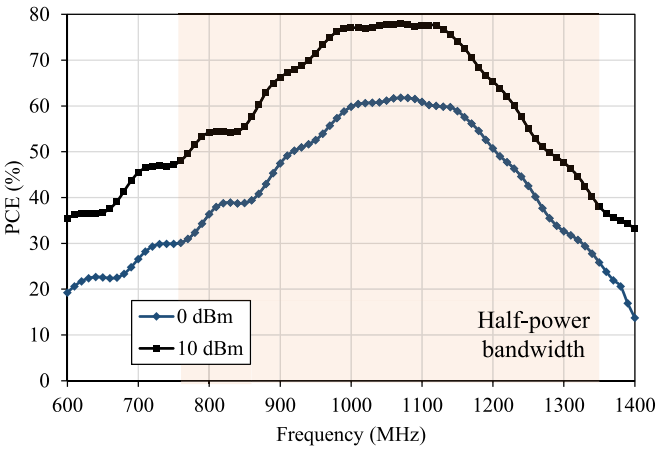

FIGURE 7. Measured PCE of the rectifier over a frequency sweep showing a 57% half-power −3 dB fractional bandwidth.

the commercially-available inductor will be lower, enabling a higher PCE. A shunt inductor, $L_2 = 47$ nH, is added to create a return path for the DC currents [43]. The value of L_2 was chosen A 0603 footprint is chosen for the inductors and the voltage doubler charge pumping 100 pF capacitors, to enable a reliable interconnect between the rectifier and the flexible e-textile filament [2]. Fig. 5 shows a close agreement between the simulated and measured input impedance of the matched rectifier, normalized to 50 Ω. The antenna's input impedance is also included in the Smith chart to show that the 50 Ω nominal impedance is maintained throughout both the antenna and the rectifier matching planes.

C. RECTIFIER EXPERIMENTAL CHARACTERIZATION

The matched rectifier was characterized using a VNA in Continuous Wave (CW) mode to investigate its performance for varying power levels, frequencies, and load impedances. Due to its CPW structure, the rectifier's performance is expected to be textile-independent, enabling it to be used for various fabrics with no limits on the thickness or the dielectric properties. In addition, the performance is expected to be maintained in human proximity. The DC output of the flexible rectifier filament was measured in space, when inserted in fabric for concealed e-textiles, and on-hand, as shown in Fig. 6.

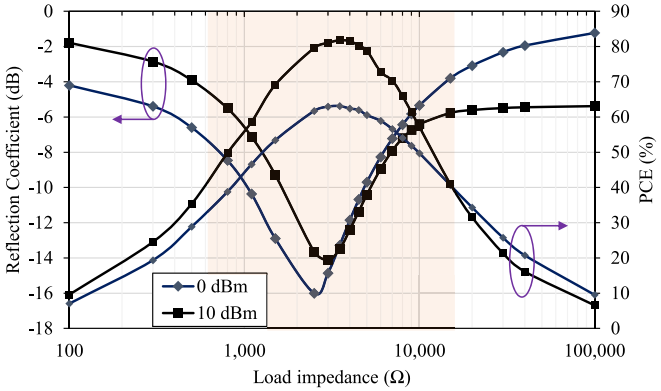

FIGURE 8. Measured reflection coefficient (S_{11}) of the rectifier for varying load impedances at 1 GHz; the shaded region indicates the half-power load range.

The frequency of the RF input power was swept at 0 and 10 dBm. Fig. 7 shows the measured PCE from 600 to 1400 MHz. It can be observed that the rectifier achieves a half-power (−3 dB) bandwidth of 57%. In addition, the rectifier achieves an approximately stable PCE above 75% from 980 to 1120 MHz at 10 dBm. The wide bandwidth demonstrates that due to the low equivalent impedance of the designed voltage doubler, a first-order matching network based on a single lumped inductor is able to result in a half-power fractional bandwidth over 50%, at the rectifier's optimal resistive load for 4.5 kΩ.

The DC output as well as the input reflection coefficient were measured to characterize the performance of the rectifier for varying load impedances. Fig. 8 shows the rectifier's measured PCE and S_{11} for varying load impedances, at 0 and 10 dBm. From the measured PCE, it can be observed that the rectifier maintains over 50% of its maximum PCE for load impedances as low as 600 Ω. A high PCE across a low-impedance load is particularly important when directly charging a capacitor without a DC-DC converter, where the equivalent series resistance of a capacitor is typically under 100 Ω.

The RF power at the rectifier's input was swept from −20 to 15 dBm, translating to approximately 0.1 to 10 m from a sub-1 GHz license-free 33 dBm EIRP source. The PCE was measured in the three test setups shown in Fig. 6, for the optimal load of 4.5 kΩ. The DC voltage was measured across both the optimal load and a 10 MΩ "open" load. Fig. 9-a and b show the simulated and measured PCE and DC voltage, respectively, at 1 GHz.

From Fig. 9-a, it can be observed that the proposed rectifier achieves over 60% PCE from 0 to 13 dBm, with a DC voltage over 1.8 V across the 4.5 kΩ optimum load. Therefore, it is expected that the rectifier can charge the TSC efficiently from under 0 dBm. Compared to recent flexible, printed, and textile-based rectifiers operating between 820 MHz and 2.4 GHz [4], [8], [12], [44], the proposed rectifier achieves the highest peak-PCE of 80%. This is attributed to the careful impedance matching using a low-value and

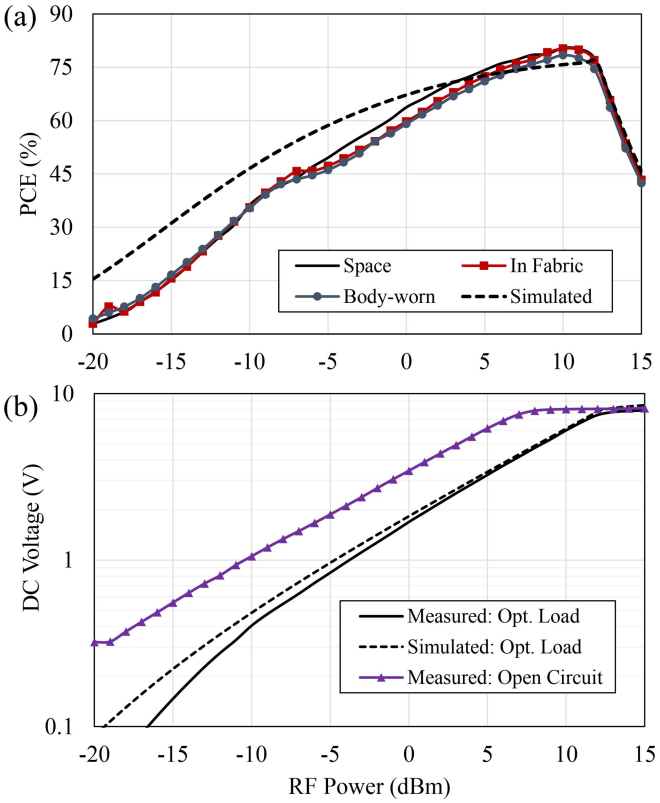

FIGURE 9. Measured (solid) and simulated (dashed) DC output of the proposed rectifier for varying power levels: (a) RF-DC PCE; (b) DC voltage.

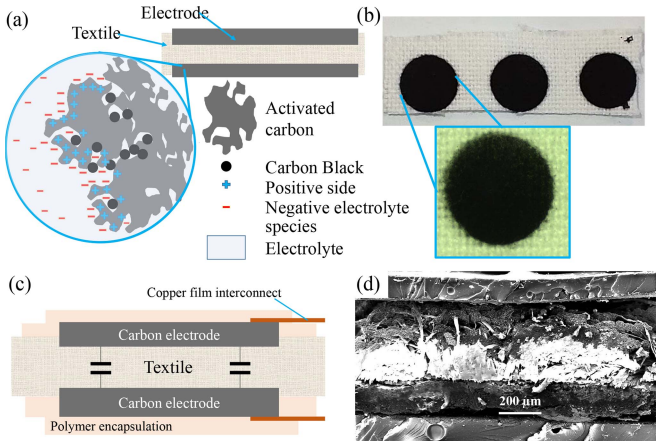

FIGURE 10. The proposed three-cell TSC: (a) 2D layout; (b) photograph and optical micrograph of the TSC cells; (c) layout of the TSC's cross-section; (d) SEM micrograph of the TSC cross-section.

high-Q lumped inductor and the distributed CPW traces. In addition, the diode selection with a relatively high breakdown voltage (V_{Br}) of 4 V and a low forward voltage of 0.25 V enables the peak-PCE improvement over [4], [8], [12], [44], which were all based on a diode with a lower V_{Br} of 2 V.

IV. TEXTILE SUPERCAPACITOR (TSC)

The TSC is composed of an aqueous electrolyte and spray-coated carbon electrodes on a conventional cotton fabric substrate. The electrode ink, formed of Ethylene-vinyl acetate (EVA), activated carbon and carbon black, was deposited using an airbrush, with a pressure of 20 psi, through a mask with 1 cm diameter holes and onto the fabric to achieve a 0.785 cm^2 electrode pair, with a mass loading of 2 mg, details of the fabrication method are presented in [18]. Activated carbon was chosen due to its high surface area and its varied pore size composition [45], the carbon black was used as a conductive additive.

The TSC was then vacuum impregnated with the electrolyte, formed of Ammonium dihydrogen phosphate (ADP) and de-ionized water. By placing the submerged TSC under vacuum, trapped air is removed and an even wetting of the electrolyte is achieved throughout the TSC. Fig. 10-a and b show the structure of the TSC sprayed on the cotton substrate. The encapsulated cross-section schematic of the TSC is shown in Fig. 10-c. Fig. 10-d shows a scanning electron microscopy (SEM) image of the cross section, demonstrating the carbon electrodes, and electrolyte-wetted cotton substrate. For simplicity of the TSC characterization, the TSC was fabricated on a separate textile substrate to that encapsulating the flexible rectenna filament. After the supercapacitors are fabricated on the textile substrate, each individual TSC cell is housed in a Swagelok test cell. This allows more reproducible measurements and guarantees a time-invariant device performance during both the DC and RF characterization.

The TSC was characterized using galvanostatic cycling (GC),, i.e., charging using a fixed DC current, and electrochemical impedance spectroscopy (EIS), to extract the equivalent circuit model of the TSC. Fig. 11 shows the measured real and imaginary impedance of the TSC from 0.1 Hz to 250 kHz, as well as the extracted equivalent circuit of the TSC. The equivalent circuit is optimized for the low frequency region as the TSC will only be charged at DC. The inset in Fig. 11-a shows the close agreement between the extracted circuit model of the TSC and the measurement. For DC charging currents between 0.25 and 3 mA/cm^2, the TSC maintains a stable aerial capacitance with less than 5% reduction in the capacitance for charging currents above 2 mA, which are unlikely to be encountered in RF-charging up to 15 dBm.

The TSC was subjected to 5 symmetric charging and discharging cycles. Due to the breakdown voltage of water, a single TSC cell is limited to 1.2 V. Nevertheless, the TSC needs to withstand the output of the rectifier, and to be able to drive electronic circuits within the supply range of low-power ICs (3.3 V to 1.2 V). Therefore, three cells are connected in series. This increases the TSC's ideal maximum voltage to 3.6 V. However, due to the purposeful simplicity of the power module no balancing circuits were utilized, hence the TSC is not charged beyond 3.2 V. Fig. 12-a shows the charging and discharging curve of the single-cell and three-cell

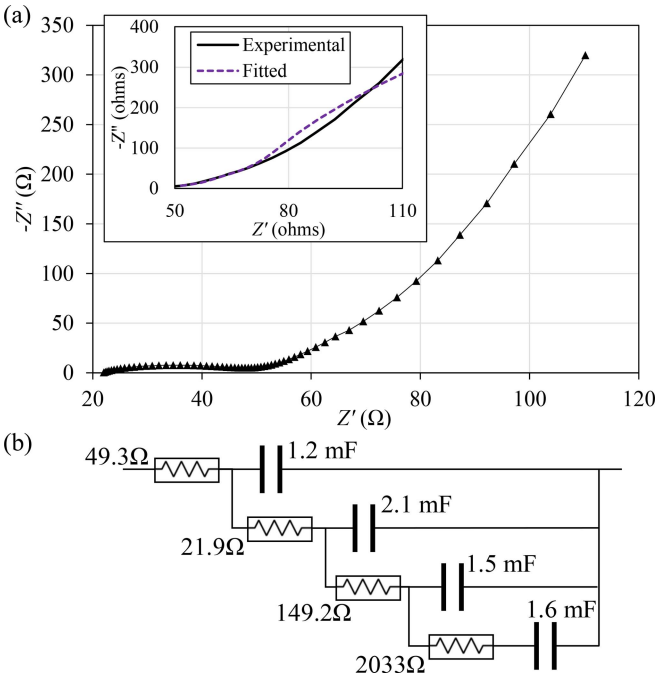

FIGURE 11. EIS equivalent model of the TSC: (a) measured and fitted real and imaginary impedance; (b) the equivalent circuit model of the three-cell TSC.

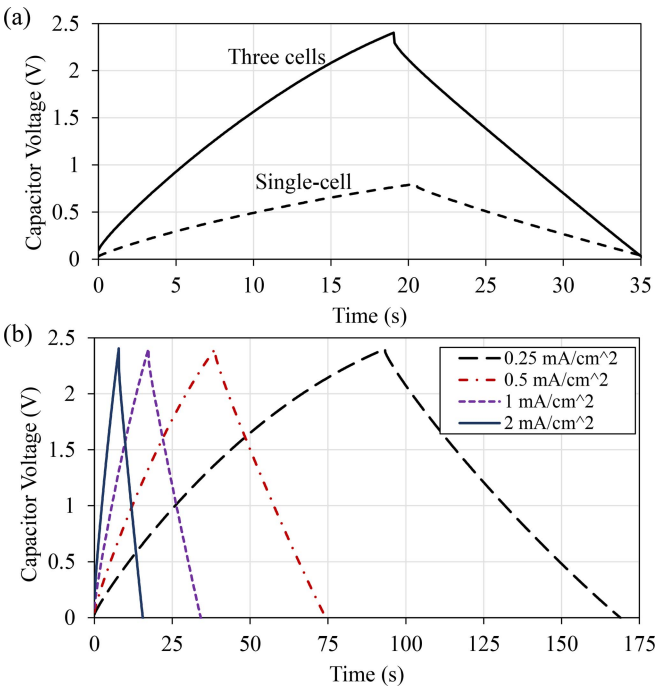

FIGURE 12. GC measurements of the TSC: (a) the single and three-cell TSC at for 1 mA/cm^2 charging current; (b) the three-cell TSC under varying current densities.

TSC from a DC current density of 1 mA/cm^2. In Fig. 12-b, the charging and discharging voltage curves are shown for DC currents between 0.20 and 1.6 mA. These values correspond to the anticipated DC output of the rectenna, for various RF power levels from 15 to 0 dBm.

The measured voltages across the capacitor during GC measurements indicate that the TSC is well-suited for integration with a rectenna. For instance, the input current of 0.2 mA (0.25 mA/cm^2) corresponds to the current driven by the proposed rectifier for P_{RF} >2 dBm, for 4.5 kΩ load. From the instantaneous voltage drop (during the current reversal) and the known measurement currents, the equivalent series resistance (ESR) of the TSC was calculated using ESR $= \Delta V/\Delta I$ as 71.9 Ω.

V. INTEGRATED RECTIFIER AND SUPERCAPACITOR EVALUATION

A. RF CHARGING AND TIME-VARIANT S-PARAMETERS

In Section III, the rectifier was characterized with a resistive load in its steady state. By using a 50 Ω RF power source, it is possible to characterize the performance of the rectifier while charging the TSC with less than 0.1 dB uncertainty in the RF power level [40]. In addition, using a VNA, it is possible to measure the single-tone time-variant s-parameters (S_{11}) of the rectifier while the capacitor is being charged.

The designed rectifier has been directly connected to the TSC to characterize the combined rectifier-supercapacitor performance. The TSC was charged for up to 180 seconds, or until the capacitor reached 2.9 V, below its voltage limit of 3.6 V. The VNA power output was swept from −4 dBm to 14 dBm, with an intermediate frequency of 10 Hz, i.e., the rectified signal resembles a 10 Hz square wave, to enable simultaneous S_{11} measurements while charging the TSC. Fig. 9 shows the voltage across the capacitor for varying RF power inputs to the rectifier.

From Fig. 13-a, it can be seen that for power levels over 0 dBm, the rectifier can fully-charge the TSC to 31.5 mJ in under 37 seconds. Below 0 dBm (Fig. 13-b), while it takes over a 100 seconds to charge the capacitor to 1 V from −4 dBm, the energy stored in the capacitor is still in excess of 3 mJ, enabling various low-power intermittent sensing and computing tasks [46]. After the maximum voltage is reached, in Fig. 13-a, the TSC is allowed to discharge freely across a 1 MΩ load. This results in a ≈2 μA current draw, the equivalent of a low-power micro-controller (e.g., TI CC2640) in sleep mode with full memory retention.

As the rectifier charges the TSC, the current drawn by the TSC varies depending on its charge level. The time-variant S_{11} of the rectifier, measured by the VNA while providing RF power to the system, enables understanding the impact of the TSC on the rectifier's impedance matching. Fig. 14 shows the measured S_{11} of the rectifier during charging, as well as the calculated equivalent DC load impedance based on the TSC charging current. The charging current was calculated using $I = C \times dV/dt$, from the measured voltage in Fig. 13-b. In this impedance calculation, it is assumed that the leakage is negligible and that all the current drawn by the TSC induces a change in the voltage across the capacitor.

At the start of the charging process, the only limit to the current drawn by the rectifier is the capacitor's ESR (71.9 Ω from the EIS measurements). In the inset in Fig. 14, it can

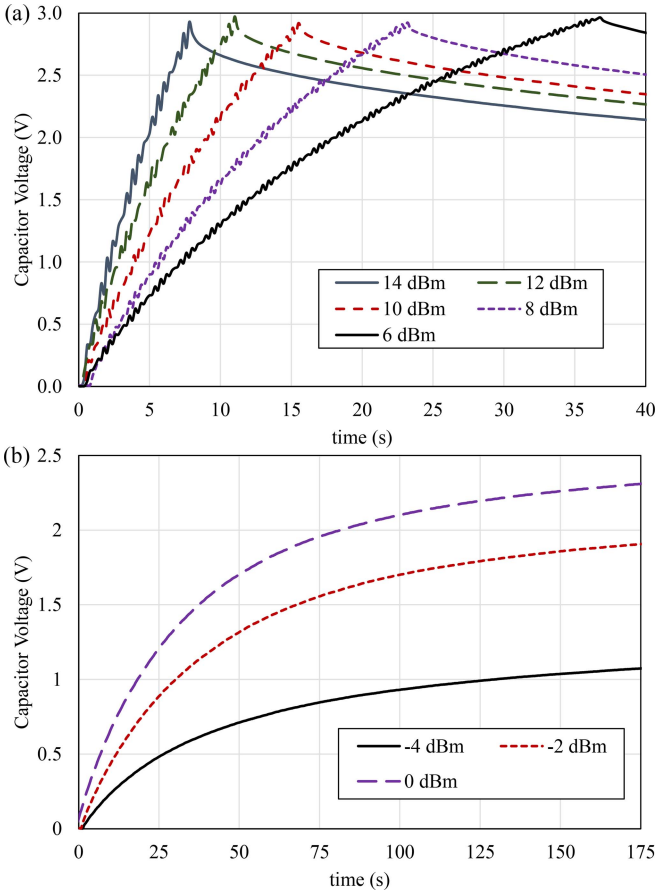

FIGURE 13. Measured voltage across the 7.5 mF textile supercapacitor for varying RF power levels: (a) >1 mW available power; (b) sub-mW power levels.

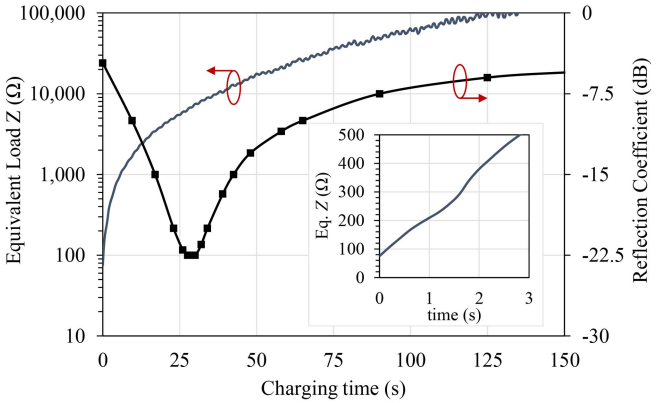

FIGURE 14. Measured S_{11} of the rectifier while charging the TSC, at 0 dBm, and the calculated equivalent load Z of the TSC; inset shows Z of the first 3 seconds.

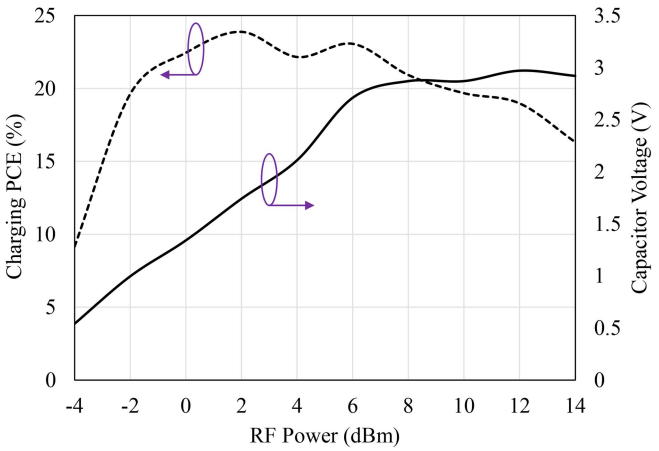

FIGURE 15. Measured voltage and average charging PCE of the capacitor for varying RF power levels, from an RF signal generator.

be seen that the equivalent load Z of the TSC, observed by the rectifier, is 74 Ω at $t = 0$, closely agreeing with the measured ESR. Recalling Fig. 8, a resistive load of 100 Ω corresponded to an $S_{11} = -4$ dB, where the measured S_{11} rectifier when charging the capacitor starts from around −5 dB. As charge builds on the capacitor, the charging current reduces and the equivalent Z lies within the optimal load impedance range of the rectifier, demonstrated by the measured S_{11} below −10 dB from 5 to 60 seconds in the charging curve in Fig. 14. While a PMIC such as TI's BQ25504 (used in [21]–[24]) would mask the variations in the load current through Maximum Power Point Tracking (MPPT), we demonstrate that the overall charging efficiency of the proposed system surpasses that of a rectifier with an MPPT boost converter PMIC, in the next subsection.

B. RECTIFIER-TSC AVERAGE CHARGING PCE ANALYSIS

The average charging power for a fixed time period t is used to evaluate the holistic PCE of the RF rectifier and TSC, based on the DC energy stored in the TSC at time t [4]. The charging PCE is given by

$$\text{PCE}_{\text{Charging}} = \frac{CV^2}{2} \times \frac{1}{t} \times \frac{1}{P_{\text{RF}}} \tag{1}$$

where C is the 7.5 mF capacitance of the three TSC cells and P_{RF} is the RF power provided by the VNA. For $P_{\text{RF}} \leq -6$ dBm, 30 seconds is chosen for t, to stay within the linear charging region of the TSC, as observed in Fig. 13. For 8 dBm and above, t is the time taken to reach 2.9 V, before the RF generator is stopped.

Fig. 15 shows the calculated $\text{PCE}_{\text{Charging}}$ and capacitor voltage at the end of the time period t. It can be observed that from −2 to 9 dBm, the $\text{PCE}_{\text{Charging}}$ is maintained above 20%, limited by the impedance mismatch between the rectifier and the TSC, the leakage of the TSC, and the rectifier approaching the breakdown voltage of the diodes beyond 8 dBm, as previously shown in Fig. 9-b. Furthermore, in 30 seconds of charging, the TSC can be charged to 1 V (3.75 mJ) from an RF input as low as −2 dBm.

The reduction in the PCE of the rectifier compared to Fig. 9-a, where an optimum resistive load was used, was previously observed with electrolytic capacitors in [4] and [25]. In [4], the average charging PCE of the capacitive-loaded rectifier was 62% lower compared to when it was terminated with an optimum resistive load. At 0 dBm, the proposed rectifier achieves an average charging PCE 60%

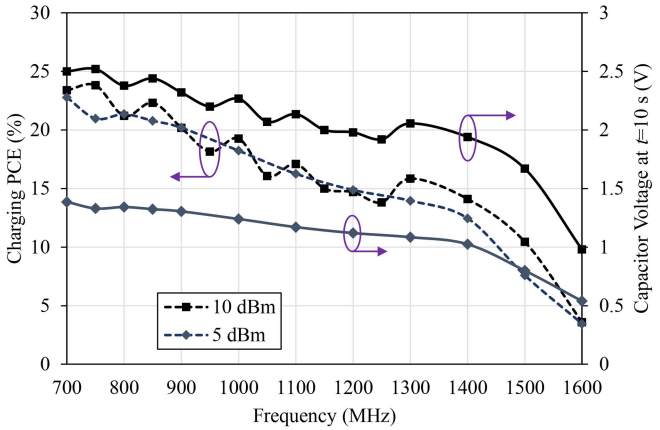

FIGURE 16. Measured charging PCE (dashed) and voltage across the capacitor (solid) for 10 s of charging, showing a 73% half-power bandwidth.

lower than the steady-state PCE observed in Fig. 9. While this work and [4] are based on different rectifier toplogies, the consistent loss in the PCE shows that the impedance mismatch effects between the storage capacitor and the rectifier are mostly consistent across different rectifiers and energy storage devices.

The TSC-loaded rectifier is then investigated for an input frequency sweep. Around 1 GHz, several frequency bands such as the 868/915 MHz ISM, 940-960 MHz GSM, and LTE/4G/5G bands down to 700 MHz are considered potential candidates for RFEH. As the resistor-loaded rectifier achieves a half-power fractional bandwidth of 57% (Fig. 7), the frequency of the Radio Frequency (RF) source was swept from 700 MHz. Fig. 16 shows the capacitor voltage after 10 seconds of charging from 700 to 1600 MHz, for a 5 and 10 dBm input.

In Fig. 16, it can be observed that the TSC-loaded rectifier achieves a half-power bandwidth of 72.7% above 700 MHz, for a center frequency of 1050 MHz, during the first 10 seconds of charging. This represents a 27.5% half-power bandwidth improvement over the resistive-loaded rectifier, previously shown in Fig. 7. It can also be seen that the high PCE is maintained at both 5 and 10 dBm. Therefore, the wider bandwidth achieved by the capacitive-loaded rectifier compared to resistive-loading (in Fig. 7) can be identified as a key benefit of directly connecting an RF rectifier to a supercapacitor.

VI. WIRELESS RECTENNA TESTING

A. DISTANCE SWEEP

In order to demonstrate the integrated rectenna and supercapacitor wireless charging module in a real-world application, a commercially-available license-free power transmitter was used to charge the capacitor at varying separations. The transmitter is a 915 MHz 3 W (34.77 dBm) Equivalent Isotropically Radiated Power (EIRP) Powercast, which uses a vertically-polarized patch antenna. As observed in Fig. 16 the TSC-loaded rectifier achieves over an octave half-power bandwidth and is therefore expected to charge

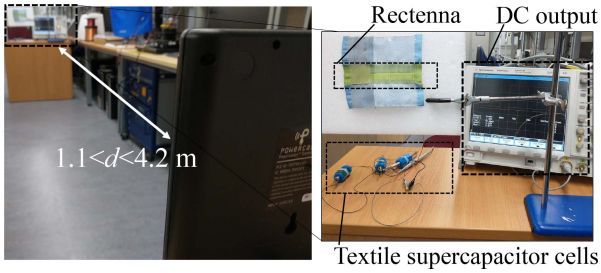

FIGURE 17. Wireless test setup of the rectenna using a 34.77 dBm 915 MHz Powercast transmitter.

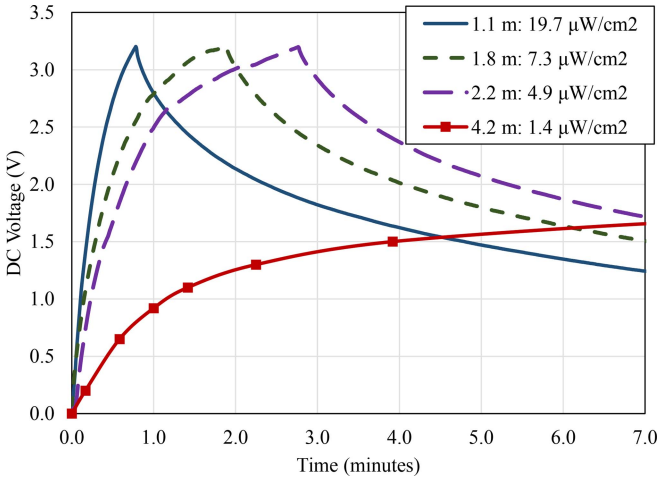

FIGURE 18. Measured voltage across the 5.6 mF capacitor during wireless charging at varying separation from the 915 MHz 34.77 dBm transmitter.

efficiently from the 915 MHz source. The rectenna was concealed inside the bespoke fabric pocket and connected to the supercapacitor cells in their Swagelok test cases using conductive silk-coated Litz threads. Fig. 17 shows a photograph of the wireless test setup of the rectenna.

Fig. 18 shows the measured DC voltage across the capacitors during wireless charging at varying distances from the Powercast transmitter. From the capacitance of 5.6 mF of the three cells used in this test, the energy stored in the capacitor is around 28 mJ in under 3 minutes at 2.2 meters from the source. This corresponds to an incident plane wave with a power density S of 4.4 μW/cm^2, calculated as in [4]. At 4.2 m away from the source ($S = 1.2$ μW/cm^2), the integrated module harvests 6.2 mJ of DC energy in 4 minutes of charging. For a high S of 17.7 μW/cm^2 ($d = 1.1$ m), the TSC is fully charged to 3.2 V (28.2 mJ) in 45 seconds.

The RF power available at the rectenna was estimated using the calculated RF power density S of the plane wave available from the transmitter [4], [21]. The power received by the rectenna is calculated using the antenna's effective area based on the measured peak gain of the antenna (Fig. 4). The peak gain is chosen to obtain a conservative estimate of the rectenna's PCE [12]. The wireless charging efficiency was calculated using (1) based on the available RF power for a charging period t of 30 seconds. Fig. 19 shows the

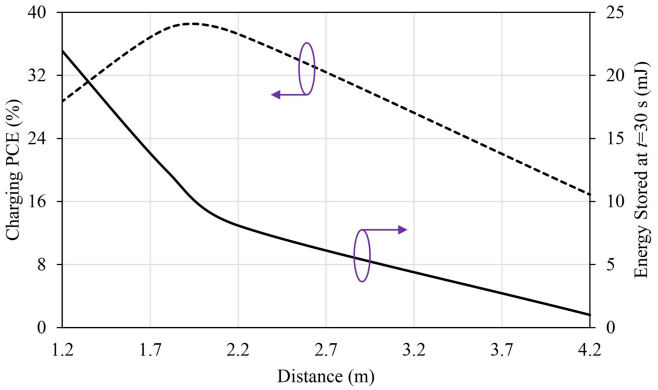

FIGURE 19. Measured energy stored in the capacitor and average charging PCE for the first 30 seconds of wireless charging for varying distance from the source.

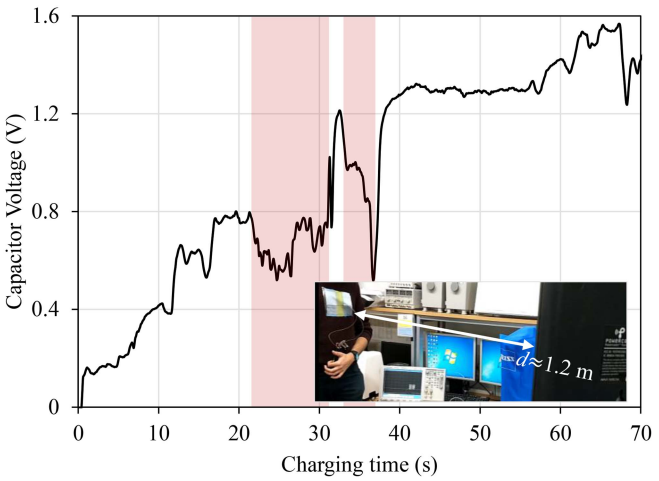

FIGURE 20. Wireless charging of the body-worn rectenna and TSC at 1.2 m from the transmitter; inset shows a photograph of the wearable test setup.

calculated end-to-end PCE of the rectenna while charging the TSC. Using this setup, the wireless charging PCE is inclusive of the mismatch losses between the antenna and the rectifier, the mismatch between the rectifier and the TSC, as well as the rectification losses and the self-leakage of the TSC. The rectenna achieves its maximum wireless charging PCE of 38% at $d = 1.8$ m from the source. Below 1.8 m, the power available at the rectenna exceeds 10 dBm and subsequently the rectifier is operating in its breakdown region and therefore the PCE reduces. At 4.2 m from the source, the proposed module achieves an end-to-end efficiency of 17% from $S = 1.35$ μW/cm^2, showing the suitability of the proposed rectenna for harvesting low RF power densities. The energy harvested in 7.1 minutes of charging from $S = 1.35$ μW/cm^2 ($d = 4.2$ m) is 10.8 mJ.

B. WEARABLE OPERATION

To demonstrate the wearable operation of the integrated e-textile energy harvesting module, the textile-concealed rectenna was placed on a user's body and connected to the TSC. The TSC was encapsulated using a heat-pressed polymer film, shown in Fig. 10-c, for bonding the three cells and providing a reliable electrical interconnect to the rectenna's output leads. Fig. 20 shows the capacitor voltage during wireless charging on the body along with a photograph of the measurement setup.

From Fig. 20, it can be seen that despite the decrease in the received power due to a degradation in the antenna's gain, which typically exceeds −4 dB, [4], and can be up to −20 dB [7], the TSC can still be charged to approximately 1.6 V in 65 seconds, at 1.2 m from the 915 MHz 34.77 dBm (EIRP) source, translating to a power density of 16.6 μW/cm^2. While charging, the effects of body shadowing were investigated through various body movements which introduce additional shadowing. The shaded regions in Fig. 20 show the time where the rectenna was covered by hand which significantly reduces the received RF power.

Despite the introduced body shadowing for about 8 seconds, from $t = 22$ to $t = 30$ s, and the lack of shielding of the proposed rectenna, the rectenna charges the TSC to 1.2 V in the first 32 seconds. This demonstrates a wearable charging efficiency of 4.8%, inclusive of the antenna losses due to human proximity, from an incident power density of approximately 16.6 μW/cm^2. Therefore, the proposed rectenna and TSC integrated module can be used both in presence and absence of the human body. While a power density of 16.6 μW/cm^2 is relatively high and may not be available from ambient sources, the proposed rectenna compares favorably with recent low-profile (sub-1 mm-thick) unshielded textile rectenna implementations that were only able to yield over 1 V DC (across a resistor in steady-state operation), from $S > 40$ μW/cm^2 at 2.9 GHz, and using as many as 81 individual rectenna cells [7].

C. COMPARISON WITH PREVIOUS WORK

The proposed energy harvesting and storage unit is compared to related work in Table 2. The charging time and DC energy are quoted at the end of the charging period. Where the average efficiency was not reported, the charging efficiency is calculated using (1) for the linear region of the charging curve, yielding the highest efficiency of the harvester in comparison.

Previously, PCB rectennas were used to charge a supercapacitor and a battery in [22] and [26], respectively. Nevertheless, in both cases, the rectifier was not designed specifically for directly charging the storage device. Therefore, their average charging efficiency is lower than the proposed rectenna-supercapacitor module. Furthermore, the power consumption of the power management stage reduces the end-to-end efficiency when the harvested DC power is under 5 mW.

The rectenna in [24] achieves a high sensitivity enabling the BQ25504 PMIC to operate from −12.6 dBm (0.8 μW/cm^2) in cold-start mode. Nevertheless, due to optimizing the system for low RF input, the end-to-end charging efficiency is very low and the complexity of the implementation makes it unsuitable for e-textiles. Where a boost

TABLE 2. Comparison with reported energy harvesters integrated with energy storage devices.

Study	Energy Harvester	Energy Storage	Implementation	DC Power management	S (μW/cm^2)	DC Energy (mJ)	Charging Time (minutes)	Average efficiency	Dimensions (mm)
This work	**Sub-1 GHz rectenna**	**Textile supercapacitor**	**Textile-based**	**None**	**6.6; 1.2**	**28.7; 8.1**	**1.8; 7**	**38%; 15%**	**115×15 (70×6.5$^\diamond$)**
[22]	Sub-1 GHz rectenna	Supercapacitor	PCB	BQ25504	12.6; 5.0	12.6; 12.6	6; 12	1.6%; 2%	110×60$^\diamond$
[25]	Sub-1 GHz rectenna	Electrolytic capacitor	PCB+whip antenna	LTC3588	23.8	0.043	0.02	25%	>100× 50 × 100‡
[24]	2.4 GHz rectenna	Electrolytic capacitor	3D-printed enclosure	BQ25504	0.8	0.12	3	1.2%	47×47×20
[26]	Sub-1 GHz rectenna	Flexible battery	PCB + 130 nm IC	boost converter	31.8*	105.9	50	11.6%	90×90$^\diamond$
[27]	Ferroelectret insole	TSC	Textile-based	None	31 μW†	0.176	60	0.16%	60×60$^\diamond$
[28]	Triboelectric yarn	TSC	Textile yarns	None	8.5 μW†	0.083	1.7	1%	30×30$^\diamond$

*Calculated from the reported distance and EIRP; †instantaneous DC power output; ‡approximated from the photographs; $^\diamond$harvester-only area

converter was not needed due to a sufficient RF input, a charging efficiency up to 25% was achieved in [25] while charging a 15 μF capacitor with a maximum range of 2.3 m. The proposed rectenna achieves around 50% higher end-to-end PCE compared to [25] in addition to occupying significantly smaller area and to being implemented using all textile-based components for the antenna and the mF-range textile supercapacitors. Therefore, it can be seen compared to other high power rectennas: [25] and [26], the proposed textile module achieves the highest end-to-end efficiency.

Compared to other textile-based energy harvesters such as mechanical ferroelectret insoles and triboelectric yarns [27], [28], the efficiency of the capacitor charging was calculated relative to the optimum DC output, due to the difficulty in estimating the mechanical power density available at the harvesters. However, it can still be seen that RFEH provides at least an order of magnitude efficiency improvement due to rectennas' low impedance. To explain, a rectenna enables charging currents in the order of 100 μA to few mA, from a power density as low as 1.2 μW/cm^2, translating to a significantly shorter charging time and a higher end-to-end efficiency. Therefore, the proposed rectenna and TSC is the only e-textile solution capable of harvesting millijoules of energy in less than 4 minutes of charging from power densities down to 1 μW/cm^2, while maintaining an overall compact and low-complexity structure.

VII. CONCLUSION

In this paper, an integrated RF-powered e-textile energy harvesting and storage module was presented based on a flexible antenna filament and a textile supercapacitor. Owing to the CPW design of the rectenna, the TSC and the rectenna can be integrated on the same textile substrate independent of the substrate's RF dielectric properties. By designing a high-voltage RF rectifier with a high PCE in the 100 μW-10 mW power range, the proposed textile-based energy harvesting and storage module achieves the highest reported end-to-end efficiency exceeding 30%, at over 2 m from a license-free power transmitter. The proposed module can store up to 10.8 mJ in 7.1 minutes of charging at 4.2 m away from a source. The capacitor-rectifier interaction was investigated using time-variant s-parameter measurements as well as large-signal and broadband end-to-end PCE measurements. It was shown that the rectifier/TSC module maintains at least 20% charging PCE from −2 to 8 dBm. Given the CPW design of the rectenna, it can be transferred to different textile substrates.

This work has demonstrated several performance gains arising from directly connecting rectennas to energy storage devices. First of all, for RF power densities above 1 μW/cm^2, a significantly higher average charging PCE can be achieved compared to rectennas utilizing a boost converter PMIC. Furthermore, we conclude that an improvement of over 27% in the half-power bandwidth of a rectifier can be achieved by directly connecting the rectifier to a supercapacitor, compared to its bandwidth with a fixed resistive load. Finally, it is concluded that long-range RF WPT is capable of driving battery-less e-textile systems with over an order of magnitude efficiency improvement over other mechanical wearable energy harvesters integrated with textile supercapacitors.

REFERENCES

[1] D. Marculescu *et al.*, "Electronic textiles: A platform for pervasive computing," *Proc. IEEE*, vol. 91, no. 12, pp. 1995–2018, Dec. 2003.

[2] A. Komolafe *et al.*, "Integrating flexible filament circuits for e-Textile applications," *Adv. Mater. Technol.*, vol. 4, no. 7, 2019, Art. no. e1900176.

[3] S. Lemey, F. Declercq, and H. Rogier, "Textile antennas as hybrid energy-harvesting platforms," *Proc. IEEE*, vol. 102, no. 11, pp. 1833–1857, Nov. 2014.

[4] M. Wagih, A. S. Weddell, and S. Beeby, "Omnidirectional dual-polarized low-profile textile rectenna with over 50% efficiency for sub-μW/cm^2 wearable power harvesting," *IEEE Trans. Antennas Propag.*, early access, Oct. 20, 2020, doi: 10.1109/TAP.2020.3030992.

[5] G. Monti, L. Corchia, and L. Tarricone, "UHF wearable rectenna on textile materials," *IEEE Trans. Antennas. Propag.*, vol. 61, no. 7, pp. 3869–3873, Jul. 2013.
[6] K. W. Lui, O. H. Murphy, and C. Toumazou, "A wearable wideband circularly polarized textile antenna for effective power transmission on a wirelessly-powered sensor platform," *IEEE Trans. Antennas Propag.*, vol. 61 no. 7, pp. 3873–3876, Jul. 2013.
[7] J. A. Estrada *et al.*, "An RF-harvesting tightly-coupled rectenna array tee-shirt with greater than octave bandwidth," *IEEE Trans. Microw. Theory Techn.*, vol. 68 no. 9, pp. 3908–3919, Sep. 2020.
[8] D. Vital, S. Bhardwaj, and J. L. Volakis, "Textile based large area RF-power harvesting system for wearable applications," *IEEE Trans. Antennas Propag.*, vol. 68, no. 3, pp. 2323–2331, Mar. 2020.
[9] M. Wagih, G. S. Hilton, A. S. Weddell, and S. Beeby, "Broadband millimetre-wave textile-based flexible rectenna for wearable energy harvesting," *IEEE Trans. Microw Theory Techn.*, vol. 68, no. 11, pp. 4960–4972, Nov. 2020.
[10] D. L. Paul, H. Giddens, M. G. Paterson, G. S. Hilton, and J. P. McGeehan, "Impact of body and clothing on a wearable textile dual band antenna at digital television and wireless communications bands," *IEEE Trans. Antennas Propag.*, vol. 61 no. 4, pp. 2188–2194, Apr. 2013.
[11] M. Wagih, A. S. Weddell, and S. Beeby, "Rectennas for RF energy harvesting and wireless power transfer: A review of antenna design [antenna applications corner]," *IEEE Antennas Propag. Mag.*, vol. 62 no. 5, pp. 95–107, Oct. 2020.
[12] M. Wagih, A. S. Weddell, and S. Beeby, "Meshed high-impedance matching network-free rectenna optimized for additive manufacturing," *IEEE Open J. Antennas Propag.*, vol. 1, pp. 615–626, 2020.
[13] N. Hillier, S. Yong, and S. Beeby, "The good, the bad and the porous: A review of carbonaceous materials for flexible supercapacitor applications," *Energy Rep.*, vol. 6, no. S5, pp. 148–156, 2020.
[14] C. Choi *et al.*, "Weavable asymmetric carbon nanotube yarn supercapacitor for electronic textiles," *RSC Adv.*, vol. 8, no. 24, pp. 13112–13120, 2018.
[15] J. Noh, C.-M. Yoon, Y. K. Kim, and J. Jang, "High performance asymmetric supercapacitor twisted from carbon Fiber/MnO_2 and carbon Fiber/MoO_3," *Carbon*, vol. 116, pp. 470–478, May 2017.
[16] Y.-F. Wang, H.-T. Wang, S.-Y. Yang, Y. Yue, and S.-W. Bian, "Hierarchical $Nico_2s_4$@ Nickel–Cobalt layered double hydroxide nanotube arrays on metallic cotton yarns for flexible supercapacitors," *ACS Appl. Mater. Interfaces*, vol. 11, no. 33, pp. 30384–30390, 2019.
[17] C. Yang *et al.*, "High-performance all-solid-state supercapacitor based on activated carbon coated fiberglass cloth using asphalt as active binder," *J. Electrochem. Soc.*, vol. 167, no. 2, 2020, Art. no. 020540.
[18] S. Yong, J. Owen, and S. Beeby, "Solid-state supercapacitor fabricated in a single woven textile layer for e-textiles applications," *Adv. Eng. Mater.*, vol. 20, no. 5, 2018, Art. no. 1700860. [Online]. Available: https://onlinelibrary.wiley.com/doi/abs/10.1002/adem.201700860
[19] J. Zhu, S.-X. Zhao, X. Wu, Y.-F. Wang, L. Yu, and C.-W. Nan, "Wrapping RGO/MoO_2/carbon textile as supercapacitor electrode with enhanced flexibility and areal capacitance," *Electrochimica Acta*, vol. 282, pp. 784–791, Aug. 2018.
[20] C. V. M. Gopi, R. Vinodh, S. Sambasivam, I. M. Obaidat, and H.-J. Kim, "Recent progress of advanced energy storage materials for flexible and wearable supercapacitor: From design and development to applications," *J. Energy Storage*, vol. 27, Feb. 2020, Art. no. 101035.
[21] A. Okba, A. Takacs, and H. Aubert, "Compact rectennas for ultra-low-power wireless transmission applications," *IEEE Trans. Microw. Theory Techn.*, vol. 67, no. 5, pp. 1697–1707, May 2019.
[22] A. Okba, D. Henry, A. Takacs, and H. Aubert, "Autonomous RFID sensor node using a single ISM band for both wireless power transfer and data communication," *Sensors*, vol. 19, no. 15, p. 3330, 2019.
[23] S. D. Assimonis, S.-N. Daskalakis, and A. Bletsas, "Sensitive and efficient RF harvesting supply for batteryless backscatter sensor networks," *IEEE Trans. Microw. Theory Techn.*, vol. 64, no. 4, pp. 1327–1338, Apr. 2016.
[24] J. Bito, R. Bahr, J. G. Hester, S. A. Nauroze, A. Georgiadis, and M. M. Tentzeris, "A novel solar and electromagnetic energy harvesting system with a 3-D printed package for energy efficient Internet-of-Things wireless sensors," *IEEE Trans. Microw. Theory Techn.*, vol. 65 no. 5, pp. 1831–1842, May 2017.
[25] P. Li, Z. Long, and Z. Yang, "RF energy harvesting for battery-less and maintenance-free condition monitoring of railway tracks," *IEEE Internet Things J.*, early access, Sep. 11, 2020, doi: 10.1109/JIOT.2020.3023475.
[26] W. Zhao, K. Choi, S. Bauman, Z. Dilli, T. Salter, and M. Peckerar, "A radio-frequency energy harvesting scheme for use in low-power ad hoc distributed networks," *IEEE Trans. Circuits Syst.*, vol. 59 no. 9, pp. 573–577, Sep. 2012.
[27] S. Yong, J. Shi, and S. Beeby, "Wearable textile power module based on flexible ferroelectret and supercapacitor," *Energy Technol.*, vol. 7, no. 5, pp. 2284–2291, 2018.
[28] K. Dong *et al.*, "A highly stretchable and washable all-yarn based self-charging knitting power textile composed of fiber triboelectric nanogenerators and supercapacitors," *ACS Nano*, vol. 11, pp. 9490–9499, Sep. 2017.
[29] M. Wagih, N. Hillier, S. Yong, A. S. Weddell, and S. Beeby, "Wearable E-textile wireless RF power supply based on a textile supercapacitor and a flexible rectenna filament," in *Proc. IEEE Int. Conf. Flexible Printable Sensors Syst.*, 2020, pp. 43–48.
[30] M. Wagih, Y. Wei, A. Komolafe, R. Torah, and S. Beeby, "Reliable UHF long-range textile-integrated RFID tag based on a compact flexible antenna filament," *Sensors*, vol. 20, no. 12, p. 3435, 2020.
[31] M. Li *et al.*, "Integration and testing of a three-axis accelerometer in a woven e-textile sleeve for wearable movement monitoring," *Sensors*, vol. 20, no. 18, p. 5033, 2020.
[32] M. Wagih, A. S. Weddell, and S. Beeby, "Sub-1 GHz flexible concealed rectenna yarn for high-efficiency wireless-powered electronic textiles," in *Proc. Eur. Conf. Antennas Propag. (EuCAP)*, 2020, pp. 43–48.
[33] C. A. Balanis, *Antenna Theory: Analysis and Design*. 3rd ed. Hoboken, NJ, USA: Wiley, 2005, p. 91.
[34] M. Wagih, Y. Wei, and S. Beeby, "Flexible 2.4 GHz sensor node for body area networks with a compact high-gain planar antenna," *IEEE Antennas Wireless Propag. Lett.*, vol. 17, no. 12, pp. 49–53, Jan. 2019.
[35] Y. H. Jung *et al.*, "A compact parylene-coated WLAN flexible antenna for implantable electronics," *IEEE Antennas Wireless Propag. Lett.*, vol. 15, pp. 1382–1385, 2018.
[36] M. Wagih, O. Cetinkaya, B. Zaghari, A. S. Weddell, and S. Beeby, "Real-world performance of sub-1 GHz and 2.4 GHz textile antennas for RF-powered body area networks," *IEEE Access*, vol. 8, pp. 133746–133756, 2020.
[37] C. Song, Y. Huang, J. Zhou, J. Zhang, S. Yuan, and P. Carter, "A high-efficiency broadband rectenna for ambient wireless energy harvesting," *IEEE Trans. Antennas Propag.*, vol. 63, no. 8, pp. 3486–3495, Aug. 2015.
[38] J. Kimionis, A. Collado, M. M. Tentzeris, and A. Georgiadis, "Octave and decade printed UWB rectifiers based on nonuniform transmission lines for energy harvesting," *IEEE Trans. Microw. Theory Techn.*, vol. 65, no. 11, pp. 4326–4334, Nov. 2017.
[39] H. J. Visser, S. Keyrouz, and A. B. Smolders, "Optimized rectenna design," *Wireless Power Transf.*, vol. 2, no. 1, pp. 44–50, Nov. 2017.
[40] S.-E. Adami *et al.*, "A flexible 2.45-GHz power harvesting wristband with net system output from −24.3 dBm of RF power," *IEEE Trans. Microw. Theory Techn.*, vol. 66 no. 1, pp. 380–395, Jan. 2018.
[41] M. Aboualalaa *et al.*, "Dual-band CPW rectenna for low inputPower energy harvesting applications," *IET Circuits Devices Syst.*, vol. 14 no. 6, pp. 892–897, 2020.
[42] X. Zhang *et al.*, "Two-dimensional MoS_2-enabled flexible rectenna for Wi-Fi-band wireless energy harvesting," *Nature*, vol. 566, pp. 368–372, Jan. 2019.
[43] C. Domnik, S. Husges, and C. Degen, "Frugal energy harvesting: Microwave energy radiated into the environment from wireless networks," *IEEE Microw. Mag.*, vol. 21, no. 1, pp. 82–87, Jan. 2020.
[44] A. Eid, J. Hester, J. Costantine, Y. Tawk, A. H. Ramadan, and M. M. Tentzeris, "A compact source–load agnostic flexible rectenna topology for IoT devices," *IEEE Trans. Antennas Propag.*, vol. 68, no. 4, pp. 2621–2629, Apr. 2020.
[45] K. V. G. Raghavendra *et al.*, "An intuitive review of supercapacitors with recent progress and novel device applications," *J. Energy Storage*, vol. 31, Oct. 2020, Art. no. 101652.
[46] D. Balsamo, O. Cetinkaya, A. R. Arreola, S. C. B. Wong, G. V. Merrett, and A. S. Weddell, "A control flow for transiently powered energy harvesting sensor systems," *IEEE J. Sensors*, vol. 20 no. 18, pp. 10687–10695, Sep. 2020.

MAHMOUD WAGIH (Graduate Student Member, IEEE) received the B.Eng. degree (Hons.) from the University of Southampton in 2018, where he is currently pursuing the Ph.D. degree.

In 2017, he worked as a Research Assistant with the University of Southampton, investigating novel differential transmission lines. In 2018, he was a Hardware Engineering Intern with Arm, Cambridge, U.K., where he was a Research Intern in 2020. He is currently a Senior Research Assistant with the University of Southampton. He has over 25 journal and conference publications and has delivered an invited webinar on these topics. His research interests lie in RF energy harvesting, wireless power transmission, and wearable antennas.

Mr. Wagih was a recipient of the Best Undergraduate Project Prize at the University of Southampton, in 2018, the Best Student Paper Award at the IEEE Wireless Power Transfer Conference in 2019, and the Best Oral Paper at PowerMEMS in 2019. He won the Best 3MT Presentation Prize (second place) at the IEEE Microwave Week, 2020. He was selected for the IEEE International Microwave Symposium Project Connect in 2019. He has acted as a Reviewer for the IEEE TRANSACTIONS ON ANTENNAS AND PROPAGATION, IEEE SYSTEMS JOURNAL, and IEEE SENSORS LETTERS and SENSORS (MDPI).

NICHOLAS HILLIER received the Master of Physics (M.Phys.) degree from the University of Southampton, in 2013, where he is currently pursuing the Ph.D. degree with the Energy Storage and its Applications Centre for Doctoral Training. His current research interests include power management of e-textiles, specifically looking to integrate super capacitors, and batteries directly into textile.

SHENG YONG received the B.Eng. degree in electrical and electronic engineering from the Imperial College London in 2011, the M.Sc. degree in micro electromechanical systems in 2012, and the Ph.D. degree in fabrication and characterization of fabric super capacitor from the University of Southampton, U.K., in 2017, where he is currently a Research Fellow with the Smart Electronics and Material Group, School of Electronics and Computer Science. His current research interests include functional material formulation for e-textile, developing energy storage device for printed e-textiles, such as super capacitor, primary and secondary batteries, and hybrid battery-super capacitor energy storage device.

ALEX S. WEDDELL (Member, IEEE) received the M.Eng. (first class Hons.) and Ph.D. degrees in electronic engineering from the University of Southampton, U.K., in 2005 and 2010, respectively.

He has over 14 years of experience in design and deployment of energy harvesting systems, and has published around 55 peer-reviewed papers in the area. He is currently a Lecturer with the Center for Internet of Things and Pervasive Systems, University of Southampton, and is involved with three projects funded by EPSRC, EU Horizon 2020, and Clean Sky 2. His main research focus is in the areas of energy harvesting and energy management for future Internet of Things devices.

STEVE BEEBY (Senior Member, IEEE) received the B.Eng. (Hons.) degree in mechanical engineering from the University of Portsmouth, Portsmouth, U.K., in 1992, and the Ph.D. degree in MEMS resonant sensors from the University of Southampton, Southampton, U.K., in 1998.

He is currently the Head of the Smart Electronic Materials and Systems Research Group and leads the U.K.'s E-Textiles Network. He is currently leading three U.K. funded research projects and has received over £16 million research funding. He is a Co-Founder of Perpetuum Ltd., a University spin-out-based upon vibration energy harvesting formed in 2004, Smart Fabric Inks Ltd., and D4 Technology Ltd. He has coauthored/edited four books, including *Energy Harvesting for Autonomous Systems* (Artech House, 2010). He has given 25 invited talks and has over 300 publications and ten patents. He has an H-Index of 52. His current research interests focus on energy harvesting, e-textiles, and the use of energy harvesting in wearable applications.

Prof. Beeby was a recipient of two prestigious EPSRC Research Fellowships to investigate the combination of screen-printed active materials with micromachined structures and textiles for energy harvesting and was also awarded a Personal Chair in 2011. He is currently the Chair of the International Steering Committee for the PowerMEMS Conference series.